Journal of
Composites Science

MDPI

Article

Influence of Glass Microfibers on the Control of Autogenous Shrinkage in Very High Strength Self-Compacting Concretes (VHSSCC)

Lucas Onghero [1,*], Marcelo Tramontin Souza [2,*], Daniel Cusson [3] and Wellington Longuini Repette [1]

[1] Graduate Program on Civil Engineering (PPGEC), Nanotechnology Applications Laboratory in Construction (NANOTEC), Federal University of Santa Catarina, Florianópolis 88040-900, SC, Brazil
[2] Graduate Program on Science, Innovation and Modeling in Materials (PROCIMM), Laboratory of Mechanical Tests and Resistance of Materials (LEMER), State University of Santa Cruz (UESC), Ilhéus 45662-900, BA, Brazil
[3] Construction Research Centre, National Research Council Canada, Ottawa, ON K1V 1J8, Canada; daniel.cusson@nrc-cnrc.gc.ca
* Correspondence: lucasjba@gmail.com (L.O.); mtsouza@uesc.br (M.T.S.)

Abstract: High-performance concrete (HPC) is widely used in infrastructure for its durability and sustainability benefits. However, it faces challenges like autogenous shrinkage, leading to potential cracking and reduced durability. Fiber reinforcement offers a solution by mitigating shrinkage-induced stresses and enhancing concrete durability. In this sense, this study investigates the use of glass microfibers to mitigate autogenous shrinkage and early-age cracking in high-strength self-compacting concrete. Samples were prepared with two water-to-binder ratios (w/b): 0.25 and 0.32; and three glass microfiber contents: 0.20%, 0.25%, and 0.30 vol.%. The concrete mixtures were characterized in the fresh state for slump flow and in the hardened state for compressive strength, static, and dynamic Young's modulus. Unrestrained and restrained shrinkage tests were also conducted in the seven days-age. The findings revealed that glass microfibers reduced the workability in mixtures with lower slump flow values (w/b of 0.25), while less viscous mixtures (w/b of 0.32) exhibited a slight improvement. Compressive strength showed a proportional enhancement with increasing fiber contents in concretes with a w/b ratio of 0.32. A contrasting trend emerged in concretes with a w/b ratio of 0.25, wherein strength diminished as fiber additions increased. The modulus of elasticity improved with fiber additions only in the matrix with a w/b ratio of 0.25, showing no correlation with compressive strength results. In shrinkage tests, the addition of glass microfibers up to specific limits (0.20% for a w/b ratio of 0.25 and 0.25% for w/b of 0.32) demonstrated improvements in controlling concrete deformation in unrestrained shrinkage analyses. Concerning cracking reduction in restrained concrete specimens, the mixtures did not exhibit significant improvements in crack prevention.

Keywords: glass microfibers; autogenous shrinkage; high-performance fiber reinforced concrete; durability; cracking

Citation: Onghero, L.; Souza, M.T.; Cusson, D.; Repette, W.L. Influence of Glass Microfibers on the Control of Autogenous Shrinkage in Very High Strength Self-Compacting Concretes (VHSSCC). *J. Compos. Sci.* **2024**, *8*, 101. https://doi.org/10.3390/jcs8030101

Academic Editor: Francesco Tornabene

Received: 25 January 2024
Revised: 13 February 2024
Accepted: 8 March 2024
Published: 12 March 2024

1. Introduction

Autogenous shrinkage arises from chemical shrinkage and self-desiccation due to cement hydration. After the initial setting, autogenous shrinkage becomes progressively restrained due to the increasing rigidity, primarily resulting from the restraint imposed by aggregates and reinforcement. This generates tensile stresses, which can lead to the formation of cracks when they surpass the material's tensile strength [1]. When quantifying autogenous shrinkage, factors such as mass fluctuations, thermal variations, and external forces are typically not considered [2]. However, it is widely acknowledged that autogenous shrinkage is chiefly influenced by the water-to-binder (w/b) ratio. Additionally, factors such as the composition and fineness of the Portland cement, as well as the curing environment (temperature and humidity), also have a significant impact on shrinkage [3].

In conventional concretes and mortars, the extraction of water from larger pores is generally considered to have minimal effects on the autogenous shrinkage phenomenon and is often deemed negligible. However, in high-performance concretes (HPCs), where lower w/b ratios are characteristic, the resulting pore refinement amplifies capillary stresses. This leads to more pronounced autogenous shrinkage at early ages compared with drying shrinkage [4,5]. The impact of the autogenous phenomenon is even more pronounced in very high-strength self-compacting concretes (VHSSCCs) due to their very low w/b ratios and the presence of reactive supplementary materials. From a practical perspective, the issue of autogenous shrinkage becomes particularly significant in mass concrete applications. This concern arises when the inner core of the concrete mixture remains in an autogenous condition, implying that it does not exchange moisture with the surrounding environment.

Concrete cracking can be initiated by restrained shrinkage forces due to internal or external constraints, under specific boundary conditions. As movements in concrete structures are often restricted by elements like floors, foundations, reinforcing bars, or other structural components, various tensile stresses develop within the concrete. These stresses can surpass the concrete's tensile strength, resulting in cracks in the structural element [6].

Extensive research has been conducted to address autogenous shrinkage in cement-based materials, exploring supplementary cementitious materials, chemical admixtures, mix design variations, and controlled curing conditions [7–11]. For a detailed discussion of mitigation techniques for autogenous shrinkage in ultra-high-performance concrete, readers are referred to [12]. This work focuses on another approach to reducing cracks in concrete structures: the incorporation of fibers.

The effectiveness of fibers depends on ensuring compatibility between the properties of the cementitious matrices and the selected fiber. This compatibility is crucial for promoting strong cohesion between materials and increasing energy absorption capacity [13]. The adhesion of fibers within the cement matrix acts as an effective bridge within cracks, playing a pivotal role in mitigating high shrinkage deformations and enhancing concrete's resistance to bending [3].

Numerous studies consistently demonstrate that adding sufficient volumes of fibers leads to a significant reduction in both shrinkage and cracking by virtue of their bridging effect [14–16]. Their impact diminishes after the concrete hardens [17,18]. Some studies investigated the effects of using polypropylene fibers on concrete shrinkage. The findings highlight a significant reduction in both autogenous and overall concrete shrinkage. Additionally, researchers have attempted to investigate the effects of diverse fibers with varying geometrical characteristics (sizes and shapes) on the cracking properties of concrete [19–22]. However, most of these studies predominantly focus on the utilization of steel fibers in high-performance concretes. There is a notable dearth of research dedicated to investigating the application of glass fibers as an alternative to steel fibers in self-compacting high-performance concrete formulations. The rationale for considering glass fibers lies in their non-corrosive nature, making them a favorable choice in environments prone to corrosion. Additionally, their non-conductive property makes them suitable for applications requiring electrical insulation. Glass fibers also exhibit resistance to chemical attack in diverse environments, and from an economic perspective, they may prove more cost-effective than metallic fibers in specific cases. As per Loukil et al. [23], the integration of glass fibers within the cementitious matrix emerges as a favorable alternative to steel-reinforced concrete, particularly in the construction of precast electrical equipment shelters and slender structural elements. While autogenous shrinkage is more critical in mass concrete applications, it can influence other types of concrete structures as well.

Apart from the limited use of glass fibers in self-compacting high-strength concretes, the second contribution of this research stems from the exploration of glass fibers integrated into concrete matrices under restrained conditions. This aspect addresses another underexplored area, particularly in the assessment of autogenous shrinkage. In this context, this paper aims to fill the existing research gap by examining how the inclusion of glass microfibers in concrete mixtures can mitigate autogenous shrinkage and early-age shrinkage-induced cracking. The investigation encompasses both unrestrained and restrained shrinkage tests, along with a comprehensive characterization of fresh state properties through slump flow testing and evaluations in the hardened state, including assessments of compressive strength and static and dynamic elastic moduli.

2. Materials and Methods

2.1. Starting Materials: Selection and Characterization

A Portland cement type III was used to produce the VHSSCC, in accordance with the requirements outlined in the ASTM C 150 standard [24]. Silica fume (having 95% purity and specific gravity of 2220 kg/m^3) was blended with cement. The blend comprised 90% cement and 10% silica fume.

The characterization of the binder constituents involved a quantitative chemical determination of the oxides, which was performed using X-ray fluorescence spectrometry (specification) with molten pellets. Table 1 shows the values of the chemical characterization of cement and silica fume.

Table 1. Results of chemical analysis of cement and silica fume. LoI means loss on ignition.

	SiO_2	Al_2O_3	K_2O	Na_2O	Fe_2O_3	TiO_2	CaO	MgO	MnO_2	P_2O_5	SO_3	LoI *
Cement	18.9	3.69	0.5	0.41	2.76	0.26	63	4.22	0.05	0.03	3.1	3.2
Silica fume	94.6	<0.04	1.3	0.49	0;06	0.06	<0.02	0.2	0.34	0.04	0.1	0.1

* Loss on ignition.

The coarse aggregates, derived from natural gravel, exhibited a particle size ranging from 4.75 to 12.5 mm, along with an apparent density of 2610 kg/m^3. The fine aggregate, composed of natural sand, featured fine quartz sand with a specific mass of 2660 kg/m^3 within the range of 0.2 to 0.6 mm. This fine aggregate was classified as medium-sized according to ASTM C33 standards [25]. Tap water was employed in the preparation of the concrete mixtures. To achieve the desired flowability, a superplasticizer admixture based on polycarboxylate, typically recommended for prefabricated self-compacting concrete, was used. This admixture possesses a specific mass of 1.04 g/cm^3 and a solids content of 30% (information obtained from the manufacturer of the admixture).

A glass microfiber, the characteristics of which are detailed in Table 2, was employed. This specific fiber type was selected due to its Young's modulus proximity with that of the ultra-high-performance concretes (40–60 GPa), a crucial factor in optimizing the compatibility and performance of the cement matrix–fiber composite [26]. Using fibers with a Young's modulus close to that of the concrete matrix helps to ensure that both the fibers and the matrix deform together under load. This compatibility in deformation reduces the likelihood of cracking and enhances the overall performance of the composite material. The dimensions of the fibers were chosen to minimize contact with the coarse aggregate.

Table 2. Characteristics of the microfiber glass according to the supplier.

Young's Modulus (GPa)	Tensile Strength (MPa)	Diameter (mm)	Length (mm)	Aspect Ratio	Strain Capacity (%)	Specific Mass (g/cm^3)
72	1698	0.02	13	650	2.0–3.5	2.68

2.2. Mix Design

This study focused on three key independent variables: the water-to-binder ratio (w/b), the content of glass fibers, and the age of hydration of the mixture. To achieve high strength and durable concrete, water-to-binder ratios of 0.25 and 0.32 by mass were selected.

The proportions of materials were carefully determined, with coarse aggregate constituting 35% of the concrete volume and the mortar comprising 30% fine aggregate and 70% paste.

To maintain stability in the mixtures, this study was performed with fiber volumes of 0.2%, 0.25%, and 0.3% relative to the volume of concrete. The desired fluidity of fresh VHSSCC was guaranteed by the polycarboxylate superplasticizer (SP), dosed at 1.54% and 0.84% (relative to the mass of the binder) for mixtures with 0.25 and 0.32 w/b, respectively. Given that the fiber content was determined relative to the volume of concrete, it resulted in some minor variations in the paste volume among the different mixtures. In terms of material proportions per cubic meter (m^3), the quantities of cement and water per m^3 exhibited slight variations corresponding to the increase in fiber content (as indicated in Table 3). Nevertheless, these discrepancies were minimal and did not seem to have any discernible impact on the test results.

Table 3. Materials proportions used to produce the concrete mixtures (kg/m^3).

Nomenclature	Contents (kg/m^3)							
	Cement	Silica Fume	Fine Sand	Medium Sand	Coarse Aggregate	Glass Microfiber	Water	SP
0.25_0%	706	78	309	202	922	0	196	12.07
0.25_0.20%	705	78	309	202	920	5.36	196	12.05
0.25_0.25%	704	78	309	202	920	6.70	196	12.04
0.25_0.30%	704	78	309	202	919	8.04	196	12.04
0.32_0%	630	70	309	202	922	0	224	5.88
0.32_0.20%	629	70	309	202	920	5.36	224	5.87
0.32_0.25%	628	70	309	202	920	6.70	224	5.86
0.32_0.30%	628	70	309	202	919	8.04	224	5.86

2.3. Test Procedures for Concrete Characterization

This section outlines the methods employed to evaluate the fresh and hardened-state properties of the concrete. These methods include the slump flow test, determination of specific mass, measurement of compressive strength, assessment of static and dynamic elastic moduli, and, finally, analysis of unrestrained and restrained shrinkage. Figure 1 summarizes the performed analysis.

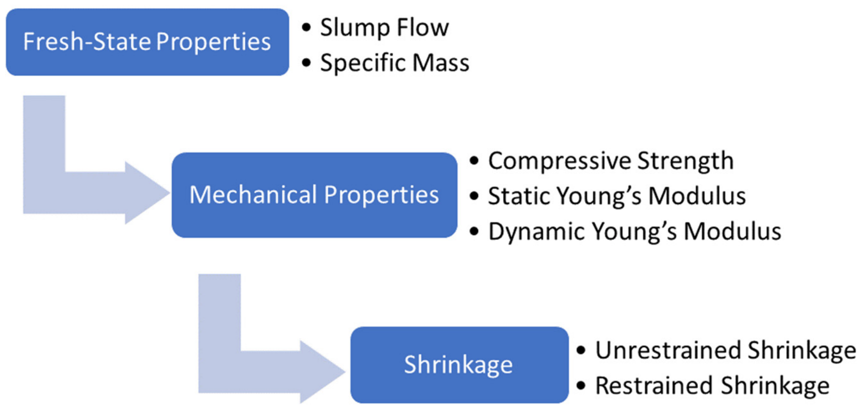

Figure 1. Flowchart of the conducted experiments.

The slump flow test was used to evaluate the flowability characteristics of the concrete mixes. The admixture dosage was adjusted for the control mix (without fibers) to achieve a slump flow exceeding the minimum requirement of 600 mm as mandated for self-compacted concrete (SCC) in compliance with ASTM C 1611 [27]. The admixture dosage was kept constant to evaluate the effect of various fiber dosages on the slump flow of the mixtures.

The concrete specific mass test was determined using the gravimetric method, following the guidelines outlined in the ASTM C 138 standard [28]. This procedure enabled the calculation of both the entrained air content introduced during the mixing process and the consumption of the materials.

Cylinders with nominal dimensions of 10 × 20 cm were used to evaluate the compressive strength, according to ASTM C39 [29]. The samples were loaded at a rate of 0.6 MPa/s. Testing was conducted at different ages, at 3, 7, and 28 days, in Shimadzu equipment with a loading capacity of 2000 kN.

The dynamic modulus of elasticity was determined according to the standard test methods ASTM C 215 [30] and ASTM E 1876 [31]. These methods establish a correlation between the material's dynamic modulus and its fundamental resonant frequency. For the static modulus test, the procedure followed the guidelines outlined in ASTM C 469 [32]. This test was conducted on the same specimens that were previously subjected to compressive strength testing. Each mixture underwent testing of dynamic and static elastic modulus on five specimens, with evaluations conducted at 3, 7, and 28 days of hydration.

Unrestrained autogenous shrinkage was performed to determine the volumetric variation exhibited by the concrete mixtures. The dimensions of the molds used were 75 mm × 75 mm × 285 mm, according to ASTM C157 [33]. Deformations were continuously measured from the first hours of hydration, with automated readings taken at five-minute intervals. For each mixture, three prisms were molded, and the longitudinal deformations were measured on both faces of the prisms (Figure 2a). A fourth prism was molded to monitor variations in the temperature and relative humidity of the concrete. The specimens were kept at 23 ± 2 °C at 50 ± 4% relative humidity throughout the test period. To ensure that there was no restriction by the mold, a double layer of plastic film was applied to the interior of each metal mold. These tests were conducted in sealed samples cured for seven days (Figure 2b).

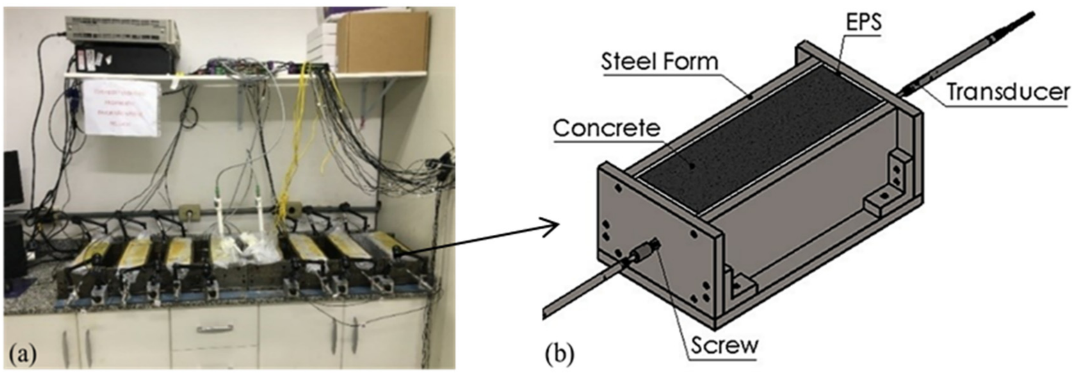

Figure 2. Photographs of (**a**) unrestrained shrinkage instrumentation and (**b**) mold details.

The restrained autogenous shrinkage test was carried out to investigate the effects of the addition of glass microfibers on cracks in restricted concrete. These cracks primarily result from the stresses caused by autogenous shrinkage. The test was performed according to ASTM C 1581 [34]. Three specimens of each mixture were prepared. Each mold was formed by two concentric steel rings measuring 330 ± 3.3 mm (internal diameter), 406 ± 3 mm (external diameter), and 152 ± 6 mm in height (Figure 3). Each inner steel ring was instrumented with three pairs of strain gauges, which were attached to the surface but not in direct contact with the concrete. The top faces of the concrete rings were promptly sealed by a polymeric acrylic-based film immediately after the molding. After 24 h, the outer metal ring was removed, and the outer side of the concrete ring was immediately painted. As for unrestrained shrinkage measurements, the deformation of the metal rings was measured at five-minute intervals and collected through a data acquisition system.

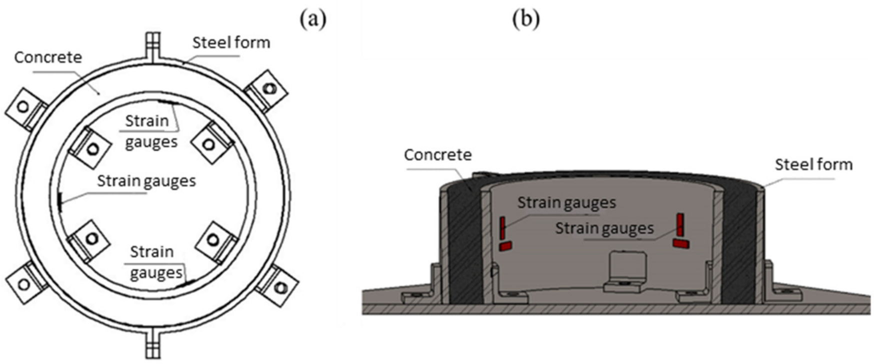

Figure 3. Illustration of the (**a**) restrained shrinkage test instrumentation and (**b**) the transversal section of mold in detail.

Figure 2a shows the specimen from above at the onset of the test, and Figure 2b shows the section of the specimen at the onset of the test.

These tests were conducted in sealed samples cured for seven days. Table 4 provides a concise summary of the conducted tests, including details about the dimensions of the test specimens, and the respective norms or standards followed for each test.

Table 4. Summary of tests performed, parameters, and standards.

Test	Specimen	Dimension [mm]		Standard
Slum Flow	Fresh state	-		ASTM C1611 [27]
Specific Mass	Fresh state	150 × 150 × 150		ASTM C 138 [28]
Compressive Strength	Cylinder	100 × 200		ASTM C39 [29]
Static Young's Modulus	Cylinder	100 × 200		ASTMC469 [32]
Dynamic Young's Modulus	Cylinder	100 × 200		ASTM E1876 [31]
Unrestrained Shrinkage	Prism	75 × 75 × 285		ASTM C157 [33]
		Inner diam.	330 ± 3.3	
Restrained Shrinkage	Ring model	Outer diam.	406 ± 3	ASTM C1581 [34]
		Height	6	

3. Results and Discussion

3.1. Fresh State Properties: Flowability, Specific Mass and Air Content

The effects of fiber addition on the fresh state properties of the mixtures are presented in Figure 3. Notably, in highly viscous mixtures (w/b = 0.25, Figure 4a), loss of fluidity occurred when the fiber was incorporated. This is because the fibers act as physical barriers that the constituents of the mixture must navigate, and their relatively large aspect ratio and specific surface area account for the decrease in fluidity. This loss of fluidity was consistent across various fiber contents, with no significant differences observed among the levels of the fiber content tested. For the w/b of 0.32 (Figure 4b), the addition of fibers did not significantly change the fluidity of the mixtures. Indeed, there was a slight increase in fluidity as the fiber content increased.

Additionally, another factor affecting workability can be a large fiber surface area. This can cause the material to behave more like a lamellar aggregate, increasing water consumption in the mixture and impacting fluidity, as well as trapping air, particularly in mixtures with low W/Wb ratios.

For both w/b ratios, a significant increase in the content of entrained air was observed during the mixing process with increasing fiber additions, leading to concretes with lower specific masses. The incorporation of air, in the absence of additives, is often attributed to the reduction in workability. During the mixing process, air is entrapped, particularly in stiffer mixes, a phenomenon well documented in the literature [35]. In fact, when comparing the reference samples with w/b ratios of 0.28 and 0.32, the fluidity is slightly higher for the w/b 0.32 sample, resulting in a lower content of entrained air. On the other hand, the mixtures with a w/b ratio of 0.32 containing fibers exhibit a different behavior, as both workability and entrained air increase with higher additions of fibers.

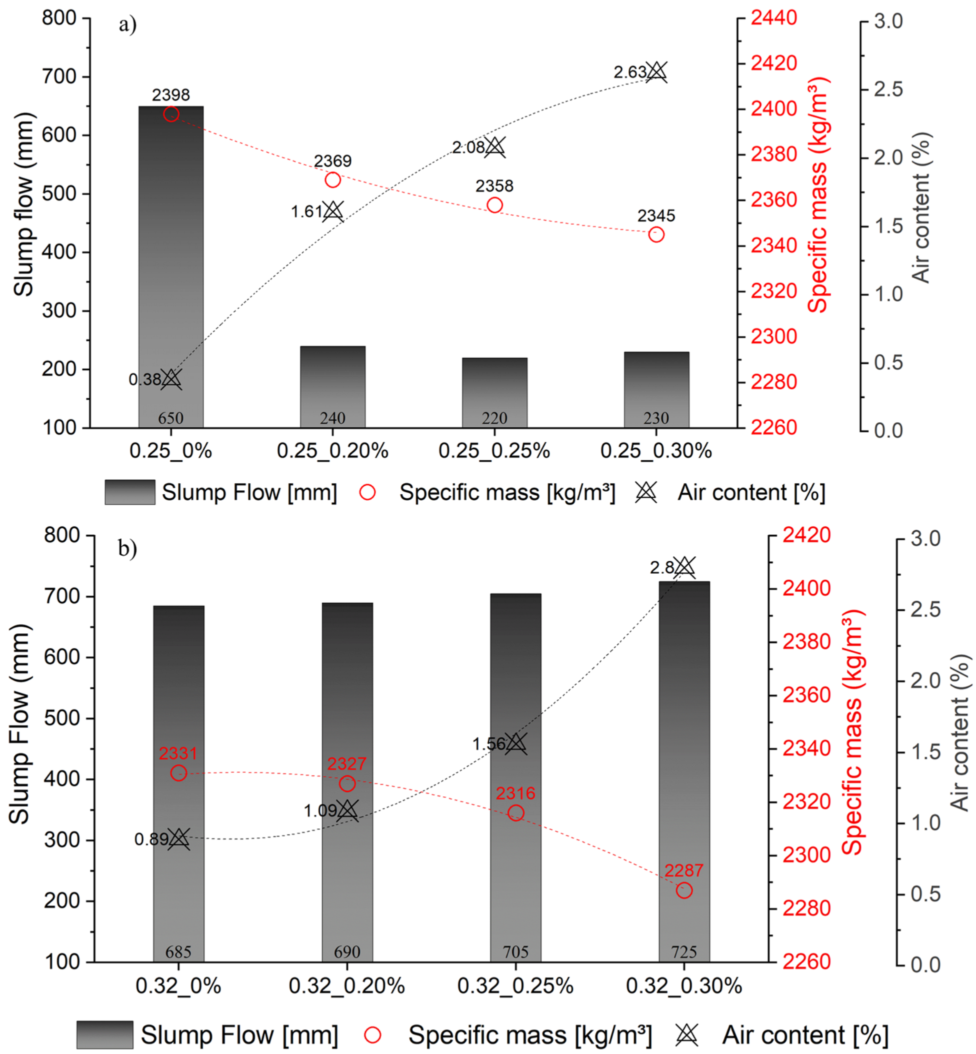

Figure 4. Results of fresh state tests (slump flow, specific mass, and entrained air) for mixtures with (**a**) w/b 0.25 mixtures and (**b**) w/b 0.32.

The literature addressing the impact of glass fibers on the workability of high-strength self-compacting concretes is limited. Thus, we conducted a comparative analysis with findings from studies on traditional self-compacting concretes with medium strength available in the literature (see Table 5). While there are no records of increased fluidity with the insertion of glass fibers, it is observed that the reduction in workability is less pronounced in some studies, while more significant in others.

The increase in fluidity with fiber additions reported in this work may be related to the interaction of fibers and additives with a higher water content, which might improve the dispersion of the fibers [36]. Rheological analysis is not the primary focus of this study; however, given the investigative gap in rheological analysis of high-strength self-compacting concretes reinforced with fibers, it can be a subject for future studies.

Table 5. Comparison of slump flow results of this work with glass-fiber reinforced concretes from literature.

Reference	Type of Concrete	SP (wt.%)	w/b Ratio	Length (mm)	Aspect Ratio	Content of Fiber (vol.% (1) or wt.% (2))	Slump Flow (mm)
This work	Very high strength self-compacting concretes	1.5	0.25	13	650	Control, 0.2, 0.25, and 0.3% (1)	650, 220, 210, and 215
		0.8	0.32				685, 690, 710, and 725
Sanjeev et al. [37]	Self-compacting concrete	1.0	0.36	6	461	Control, 0.02, 0.03 and 0.04% (1)	740, 720, 700, and 680
Hake et al. [38]	Self-compacting concrete	2.5	0.54	12	857	Control, 0.25 and 0.5% (2)	689, 681, and 676
Ahmad et al. [39]	Self-compacting concrete	0.8	0.35	12		Control and 0.025 (2)	720 and 710
Güneyisi et al. [40]	Self-compacting concrete	0.21–0.28	0.35	12	923	Control, 0.35 and 0.7 (1)	~745 and ~730
Mehdipour et al. [41]	Self-compacting concrete	0.5	0.35	6	150	Control, 0.1, 0.2, and 0.5% (1)	46, 45, 43, and 38 *
				12	200	Control and 0.5% (1)	46 and 36 *
Ghosh et al. [42]	Self-compacting concrete	0	0.62	19	106	Control and 0.3% (1)	678 and 531
				12.7	71		678 and 546

* They used mini-slump flow tests. (1) Percentage of concrete volume; (2) Percentage of the binding weight.

At this moment, it is worth highlighting the guidelines set forth by The European Guidelines for Self-Compacting Concrete (EFNARC) [43], which categorizes the standard slump flow for a diverse range of applications into three distinct classes. SF1 represents spreading in the range of 550 to 650 mm, SF2 for 660 to 750 mm, and SF3 for 760 to 850 mm. According to EFNARC's recommendations, SF1 (550–650 mm) is apt for applications involving unreinforced or slightly reinforced concrete structures that are cast from the top, allowing for free displacement from the delivery point (e.g., housing slabs), as well as for casting via a pump injection system (e.g., tunnel linings). It is also suitable for sections small enough to prevent long horizontal flow (e.g., piles and certain deep foundations). SF2 (660–750 mm) is well suited for a multitude of standard applications, including walls and columns. On the other hand, SF3 (760–850 mm) is specifically recommended for vertical applications within highly congested structures, those with complex shapes, or when filling under formwork is required.

Thus, by following the EFNARC guidelines, the control mixture with a w/b of 0.28 falls within the SF1 class, nearing the upper limit. However, mixtures with the same w/b ratio incorporating fibers do not meet the criteria for classification as self-consolidating concretes. Conversely, all mixtures with a w/b ratio of 0.32 are assigned to the SF2 class.

3.2. Mechanical Properties

Figure 5 depicts the results obtained from compressive tests. Notably, in the case of fiber-reinforced concretes with a w/b of 0.25 (Figure 5a), there is an evident decline in the average mechanical performance corresponding to the increase in the fiber content. In contrast, for a w/b ratio of 0.32 (Figure 5b), a remarkable strengthening effect can be observed with increasing fiber additions, particularly pronounced at 28 days.

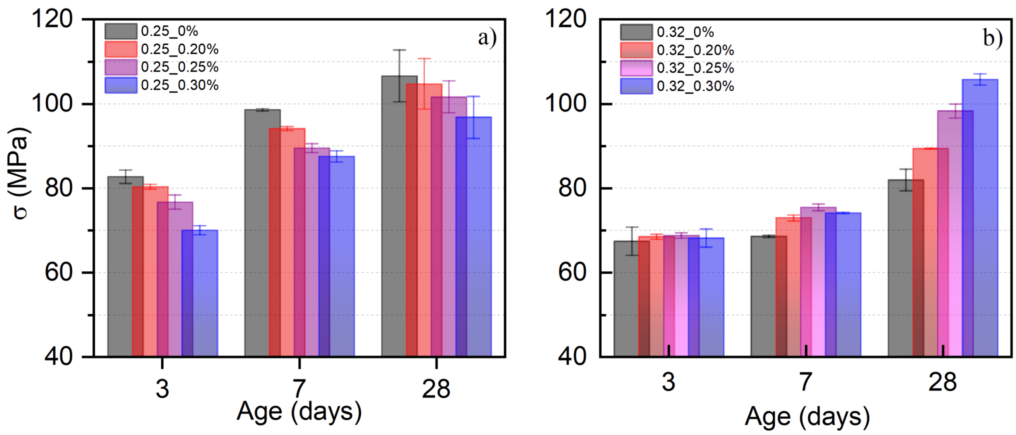

Figure 5. Results of compressive tests for mixtures with (**a**) w/b 0.25 mixtures and (**b**) w/b 0.32.

Hence, the influence of fibers on compressive strength is contingent on both the fiber content and the w/b ratio. In the case of very high-performance concretes, typically presenting compressive strengths surpassing 100 MPa after 28 days of curing, the impact of fibers is detrimental to mechanical strength, which diminishes with increasing fiber content. Conversely, for higher w/b ratios, where concretes do not exceed 100 MPa, the fiber effect is beneficial, progressively enhancing strength in proportion to the fiber content employed.

As for comparison, Schwartzentruber et al. [1] observed a 19% reduction in slump flow and a slight improvement in compressive strength at 28 days by incorporating 1% volume of glass fibers with similar dimensions and an aspect ratio in ultra-high strength mortar (with a water-to-binder ratio of 0.25). Similar trends were observed with other types of microfibers [44]. Kumar et al. [45] reported an increase in compressive strength up to a certain threshold content (~0.3 vol.%). Beyond this threshold, there was a noticeable decline in compressive strength. This finding was also noticed by Loukil et al. [23] The authors attributed this loss of compression strength to less compaction of the material associated to spaces occupied by the glass fibers.

Table 6 summarizes our research findings and provides a comparative analysis with results reported in the existing literature. It can be noticed that for all self-compacting concretes, the compressive strength rises with increasing glass fiber additions. These findings suggest that the fiber dispersion and workability are the primary factors influencing the mechanical performance of concretes.

Table 6. Comparison of compressive strength results of this work with glass-fiber-reinforced concretes from literature.

Reference	Type of Concrete	w/b Ratio	Aspect Ratio	Content of Fiber (vol.% (1) or wt.% (2))	Compressive Strength at 28-Days Age (MPa)
This work	Very-high strength	0.25	650	Control, 0.2, 0.25, and 0.3 (1)	107, 105, 102 and 97
		0.32			82, 89, 98 and 106
Schwartzentruber et al. [1]	Ultra-high-performance	0.26	857	Control and 1.0 (1)	~135 and ~138
Kumar et al. [45]	High performance	0.3	857	Control, 0.33 and 0.67 (1)	30.1, 41.3, and 32.2
Loukil et al.	High performance	0.3	857	Control, 2.0 and 3.0 (2)	82, 86, and 79

Table 6. *Cont.*

Reference	Type of Concrete	w/b Ratio	Aspect Ratio	Content of Fiber (vol.% [(1)] or wt.% [(2)])	Compressive Strength at 28-Days Age (MPa)
Sanjeev et al. [37]	Self-compacting	0.36	461	Control, 0.02, 0.03 and 0.04 [(1)]	47.7, 50.2, 53.7, and 57.3
Hake et al. [38]	Self-compacting	0.54	857	Control, 0.25 and 0.5 [(2)]	39.1, 40.2, and 44.0
Ahmad et al. [39]	Self-compacting	0.35		Control and 0.025 [(2)]	45 and 47
Mehdipour et al. [41]	Self-compacting	0.35	150	Control, 0.1, 0.2, and 0.5 [(1)]	55, 55, 54, and 54
			200	Control and 0.5 [(1)]	55 and 56

[(1)] Percentage of concrete volume; [(2)] Percentage of the binding weight

Figure 6 shows the static modulus and the dynamic elastic modulus of the specimens. For the mixture with a w/b of 0.25 (Figure 6a,c), both static and dynamic elastic moduli are less influenced at early ages but demonstrate a clear improvement with fiber incorporation at 28-days age. At this age, the mixture with w/b = 0.32 demonstrated minimal variation in values (refer to Figure 6b,d). This contrasts with the findings in compressive strength, where a w/b of 0.32 improved with the influence of fibers. Given that both elastic and dynamic modulus values were derived from distinct test procedures, the convergence of results toward the same tendency suggests the improbability of testing errors. The consistency of these findings is further emphasized by the significantly higher correlation observed between the outcomes of both analyses, as illustrated in Figure 6e.

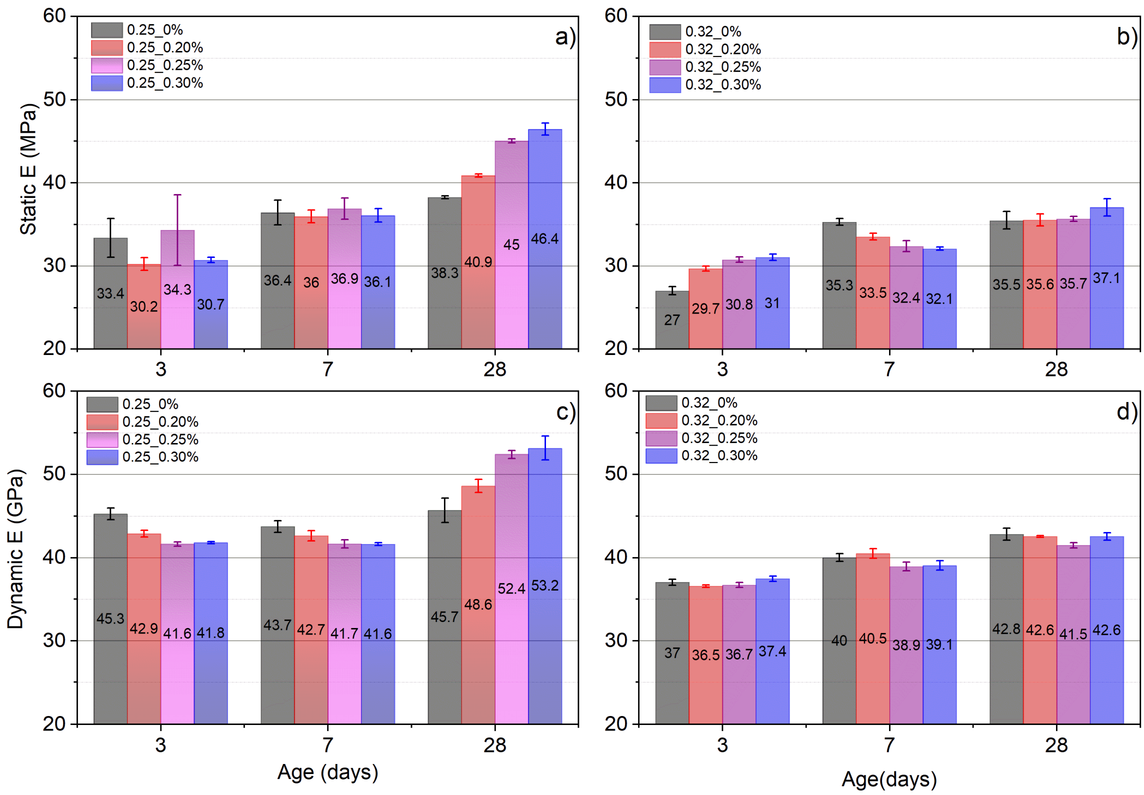

Figure 6. *Cont.*

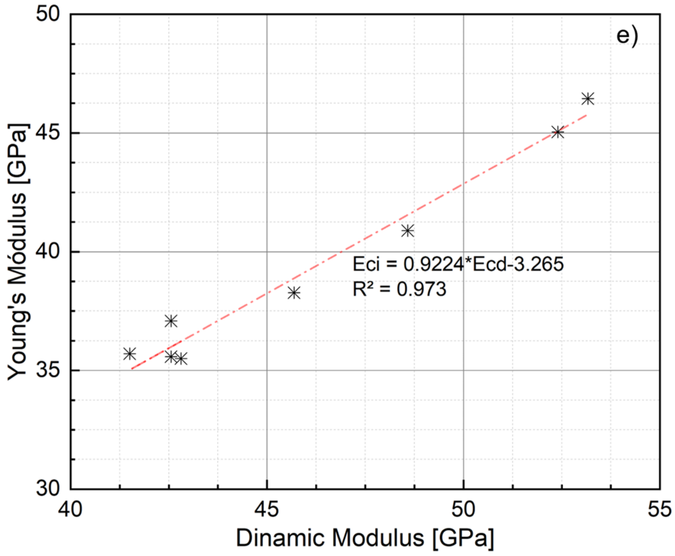

Figure 6. Results of static modulus for mixtures with (**a**) w/b 0.25 and (**b**) w/b 0.32 ratios and of dynamic modulus for mixtures with (**c**) w/b 0.25 and (**d**) w/b 0.32 ratios; (**e**) shows the correlation between static and dynamic moduli of elasticity data at 28-day age.

It has been reported that fibers have a lesser impact on the modulus of elasticity of concrete in compression [46], yet they exhibit the potential to enhance the modulus of elasticity in tension [47]. Nevertheless, this observation has sparked contradictions found throughout the literature. Kumar et al. [45], Schwartzentruber et al. [1], and Abdullah and Jallo [48] have reported an uptick in the elastic modulus of concrete with the incorporation of fibers. In contrast, Kizilkanat et al. [49] documented a slight decrease in the elastic modulus with the inclusion of fibers ranging from 0.25 to 1.0 vol.%. Simultaneously, they observed enhancements in both flexural strength and split tensile strength for the corresponding fiber contents. Furthermore, while the compressive strength showed no significant impact at 0.25 and 0.5 vol.%, a slight increase was evident at 0.75 and 1.0%.

Therefore, it is evident that the results of mechanical strength tests may not always align with the outcomes of elasticity modulus tests. The underlying reasons for the disparities in findings between the present study and Kizilkanat et al., as well as their divergence from other literature, remain elusive. This discrepancy necessitates thorough exploration in future research.

3.3. Autogenous Shrinkage

The results of the unrestrained autogenous shrinkage tests are shown in Figure 7, where the mean strain of each specimen is shown over 7 days. The unrestrained shrinkage deformations obtained in the tests decreased when microfibers were added to the mixture compared with the reference sample; however, no significant differences were observed among the contents tested. This finding was consistent across both w/b ratios.

Figure 8 presents the average unrestrained autogenous shrinkage values for each concrete studied at 7 days ages. The maximum reduction in the deformation obtained in the mixtures studied was 48% for the mixture 0.25_0.20% and 75.5% for 0.32_0.25%. These contents represent the threshold limit, as higher amounts appear to diminish the effectiveness of shrinkage mitigation. This behavior has also been reported in the literature. Mehdipour et al. [41] systematically examined the influence of glass fibers on the unrestrained drying shrinkage of self-compacting concrete. Their investigation revealed a notable reduction in shrinkage with an escalation in the fiber content up to a critical threshold. This threshold is contingent upon the aspect ratio, approximately 4 vol.% for fibers characterized by an aspect ratio of 200 and approximately 6 vol.% for fibers with an aspect ratio of 150. Beyond this specified content, the diminishing returns on shrinkage reduction were noted. The researchers postulated that beyond this critical threshold, fibers exhibit insufficient distribution and interconnectivity, hindering their efficacy in stress transfer.

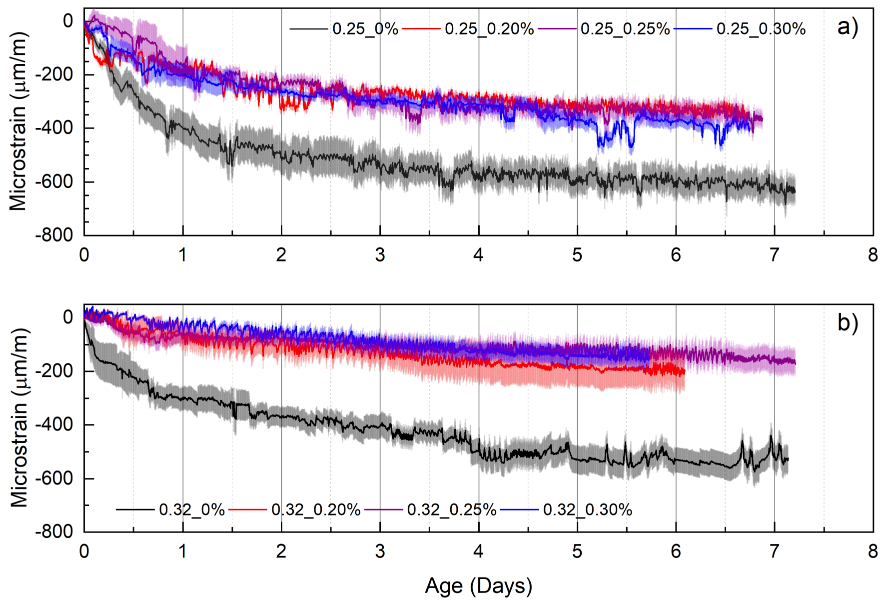

Figure 7. Unrestrained shrinkage results for mixtures with (**a**) 0.25 and (**b**) 0.32 ratios.

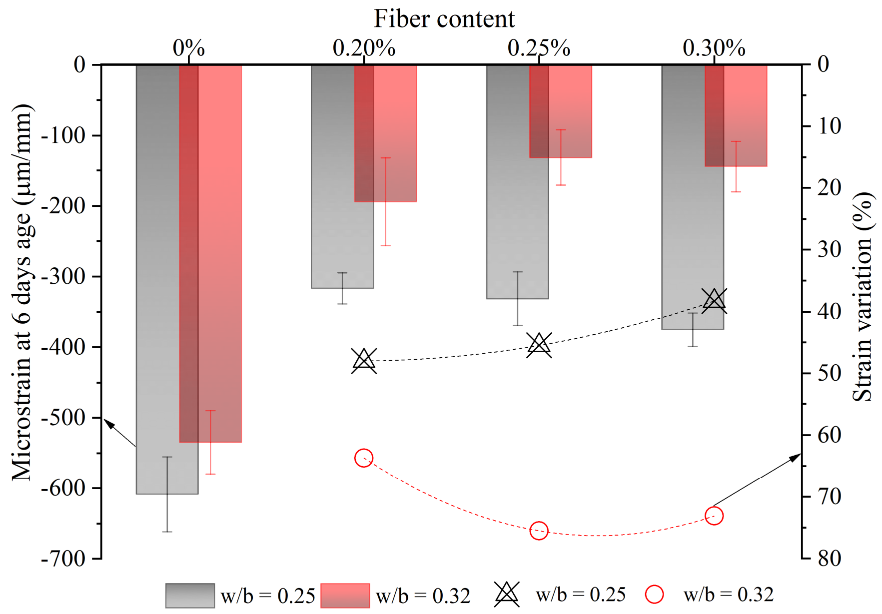

Figure 8. Microstrain measurements of unrestrained shrinkage and strain variation in concretes with different fiber contents at 7 days age.

Barluenga et al. [50] observed a significant reduction, ranging from 55% to 95%, in unrestrained cracking for two types of glass fibers tested at a concentration of 600 g/m^3. The effectiveness of cracking control diminished when both types of fibers were added at a higher concentration of 1000 g/m^3. This optimal behavior was consistently observed in restrained concrete as well, where the addition of fibers at 600 g/m^3 resulted in a substantial reduction of 70–80%.

The results of the restrained shrinkage tests are presented in Figure 9. Fiber-reinforced concrete reduced steel deformation of the ring, which indicates a reduction in concrete shrinkage, resulting in less tension generated by the restraint from the steel ring. Figure 10 depicts the timeline (in days) when cracks emerge in the samples. It is worth noting that the occurrence of cracking took place between the fourth and seventh days. However, there is no discernible correlation between the timing of cracking and the presence or content of glass fibers. This lack of correlation aligns with findings from other works. Schwartzentruber et al. [1] demonstrated a notable 24% decrease in restrained stress after incorporating approximately 1 vol% glass fibers for a 24-h period. However, the reduction in the propensity for cracking was not as substantial. Messan et al. [51] demonstrated that the addition of glass fibers at 0.06 mass% does not alter the increase in restrained tensile stress compared with the unmodified formulation. However, it significantly reduces both unrestrained shrinkage and local strain activity at the drying surface of the mortar.

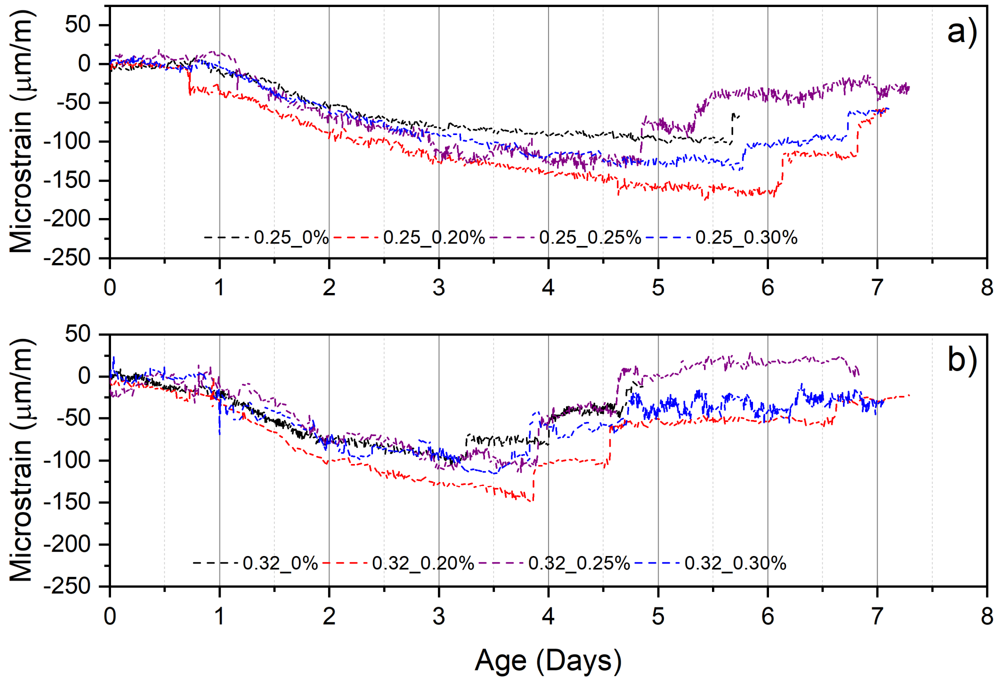

Figure 9. Microstrain measurements of restrained shrinkage of all concrete mixtures up to the seventh day (**a**,**b**).

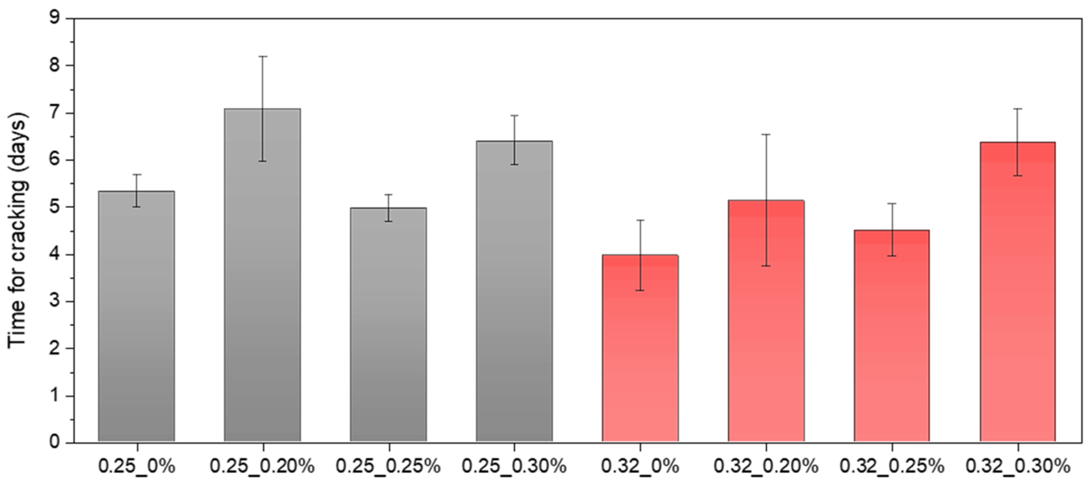

Figure 10. Time for cracking of samples in restrained condition.

4. Conclusions

This study conducted a comprehensive investigation into the effects of fiber addition on the properties of VHSSCC prisms. The assessment covered the influence of microfibers on concrete workability, mechanical properties, and both unrestrained and restrained shrinkage. The analysis of the findings leads to the following conclusions:

- ✓ Glass microfibers decreased workability in mixtures with lower slump flow values (w/b of 0.25). Conversely, in less viscous mixtures (w/b of 0.32), there was a slight improvement in slump values.
- ✓ The compressive strength demonstrated a proportional enhancement with rising fiber contents in concretes featuring a w/b ratio of 0.32. Conversely, a contrasting behavior was noted for concretes with a w/b of 0.28.
- ✓ The modulus of elasticity demonstrated improved results with fiber additions in the matrix with a w/b ratio of 0.28, showing no correlation with compressive strength results.
- ✓ In the shrinkage tests, the addition of glass microfibers, up to a certain limit, showcased improvements in controlling concrete deformation in unrestrained analyses.
- ✓ Regarding cracking reduction in restrained concrete specimens, the mixtures did not exhibit significant improvements in crack prevention.
- ✓ According to the results obtained, for the level of strengths achieved, glass microfiber does not prove effective in combating concrete cracking, even though it reduces deformation due to shrinkage in the mixtures. This shows that fiber anchorage in the matrix must be improved to increase its performance and enable its practical use.

Finally, it is worth highlighting that reducing concrete deformation with the usage of glass fibers offers numerous practical advantages. Firstly, it enhances the durability of concrete structures, extending their service life. Additionally, minimizing deformation contributes to an improved aesthetic appearance by preserving the quality of the concrete surface, enhancing the overall visual appeal of the structure. While the usage of fibers requires the addition of a superplasticizer to maintain workability, which increases the cost of concrete, minimizing concrete deformation still results in cost savings by reducing the need for frequent repairs and maintenance, which can be financially burdensome.

It is also important to point out that the effectiveness of glass fibers in reducing shrinkage might come at the expense of reducing the strength of concrete when the water-to-binder (w/b) ratio is quite low, such as 0.25 or less, as evidenced in this study. Therefore, future research can focus on assessing the influence of glass fibers in ultra-high-performance concrete, exceeding 150 MPa, where the w/b ratio can be as low as 0.20.

Author Contributions: Conceptualization, L.O. and W.L.R.; Methodology, L.O. and W.L.R.; Investigation, L.O.; Resources, W.L.R.; Data curation, L.O.; Writing—review & editing, L.O., M.T.S., D.C. and W.L.R.; Project administration, W.L.R. All authors have read and agreed to the published version of the manuscript.

Funding: This research received no external funding.

Data Availability Statement: The data presented in this study are available in article.

Acknowledgments: We would like to acknowledge the staff of the Laboratory of Application of Nanotechnology in Civil Construction (LabNANOTEC/UFSC) for their invaluable assistance. The contribution of the anonymous reviewers is also deeply acknowledged. The authors gratefully acknowledge the Brazilian governmental research agencies, the National Council for Scientific and Technological Development (CNPq), and the Coordination for the Improvement of Higher Education Personnel (CAPES) for providing financial support for this research.

Conflicts of Interest: The authors declare no conflict of interest.

References

1. Schwartzentruber, A.; Philippe, M.; Marchese, G. Effects of PVA, glass and metallic fibers, and of an expansive admixture on the cracking tendency of ultrahigh strength mortar. *Cem. Concr. Compos.* **2004**, *26*, 573–580. [CrossRef]
2. Tazawa, E.I.; Sato, R.; Sakai, E.; Miyazawa, S. Work of JCI committee on autogenous shrinkage. In *International RILEM Workshop on Shrinkage of Concrete*; RILEM Publications SARL: Pairs, France, 2000; pp. 21–33.

3. Liu, L.; Wang, X.; Chen, H.; Wan, C. Microstructure-based modelling of drying shrinkage and microcracking of cement paste at high relative humidity. *Constr. Build. Mater.* **2016**, *126*, 410–425. [CrossRef]
4. Cook, R.A.; Hover, K.C. Mercury porosimetry of hardened cement pastes. *Cem. Concr. Res.* **1999**, *29*, 933–943. [CrossRef]
5. Cusson, D.T.H.; Hoogeveen, T. An Experimental approach for the analysis of early-age behaviour of high-performance concrete structures under restrained shrinkage. *Concrete* **2007**, *37*, 200–209. [CrossRef]
6. Barr, B.; Hoseinian, S.; Beygi, M. Shrinkage of concrete stored in natural environments. *Cem. Concr. Compos.* **2003**, *25*, 19–29. [CrossRef]
7. Park, J.J.; Kim, S.W.; Ryu, G.S.; Lee, K.M. The influence of chemical admixtures on the autogenous shrinkage ultra-high performance concrete. *Key Eng. Mater.* **2011**, *452–453*, 725–728. [CrossRef]
8. Masoule, M.S.T.; Ghahremaninezhad, A. Effect of Poly(ethylene glycol)–Poly(propylene glycol) Triblock Copolymers on Autogenous Shrinkage and Properties of Cement Pastes. *Buildings* **2024**, *14*, 283. [CrossRef]
9. Golewski, G.L. The Effect of the Addition of Coal Fly Ash (CFA) on the Control of Water Movement within the Structure of the Concrete. *Materials* **2023**, *16*, 5218. [CrossRef]
10. Ghanem, H.; Ramadan, R.; Khatib, J.; Elkordi, A. A Review on Chemical and Autogenous Shrinkage of Cementitious Systems. *Materials* **2024**, *17*, 283. [CrossRef]
11. Rasoolinejad, M.; Rahimi-Aghdam, S.; Bažant, Z.P. Prediction of autogenous shrinkage in concrete from material composition or strength calibrated by a large database, as update to model B4. *Mater. Struct. Constr.* **2019**, *52*, 33. [CrossRef]
12. Yang, L.; Shi, C.; Wu, Z. Mitigation techniques for autogenous shrinkage of ultra-high-performance concrete—A review. *Compos. Part B Eng.* **2019**, *178*, 107456. [CrossRef]
13. Safdar, M.; Matsumoto, T.; Kakuma, K. Flexural behavior of reinforced concrete beams repaired with ultra-high performance fiber reinforced concrete (UHPFRC). *Compos. Struct.* **2016**, *157*, 448–460. [CrossRef]
14. Sahinagic-Isovic, M.; Arangelovski, T.; Cecez, M. Influence of steel fiber addition on the shrinkage of ordinary strength and high strength concrete. In Proceedings of the RILEM International Workshop on Performance-Based Specification and Control of Concrete Durability, Zagreb, Croatia, 11–13 June 2014; pp. 623–631.
15. Zheng, X.; Ji, T.; Easa, S.M.; Zhang, B.; Jiang, Z. Tensile basic creep behavior of lightweight aggregate concrete reinforced with steel fiber. *Constr. Build. Mater.* **2019**, *200*, 356–367. [CrossRef]
16. Shen, D.; Liu, X.; Li, Q.; Sun, L.; Wang, W. Early-age behavior and cracking resistance of high-strength concrete reinforced with Dramix 3D steel fiber. *Constr. Build. Mater.* **2019**, *196*, 307–316. [CrossRef]
17. Yoo, D.Y.; Shin, H.O.; Yang, J.M.; Yoon, Y.S. Material and bond properties of ultra high performance fiber reinforced concrete with micro steel fibers. *Compos. Part B Eng.* **2014**, *58*, 122–133. [CrossRef]
18. Altoubat, S.; Rieder, K.-A.; Junaid, M.T. Short- and long-term restrained shrinkage cracking of fiber reinforced concrete composite metal decks: An experimental study. *Mater. Struct.* **2017**, *50*, 140. [CrossRef]
19. Kakooei, S.; Akil, H.M.; Jamshidi, M.; Rouhi, J. The effects of polypropylene fibers on the properties of reinforced concrete structures. *Constr. Build. Mater.* **2012**, *27*, 73–77. [CrossRef]
20. Saje, D.; Bandelj, B.; Šušteršič, J.; Lopatič, J.; Saje, F. Shrinkage of Polypropylene Fiber-Reinforced High-Performance Concrete. *J. Mater. Civ. Eng.* **2011**, *23*, 941–952. [CrossRef]
21. Mazzoli, A.; Monosi, S.; Plescia, E.S. Evaluation of the early-age-shrinkage of Fiber Reinforced Concrete (FRC) using image analysis methods. *Constr. Build. Mater.* **2015**, *101*, 596–601. [CrossRef]
22. Sarmiento, E.V.; Hendriks, M.A.N.N.; Geiker, M.R.; Kanstad, T. Modelling the influence of the fibre structure on the structural behaviour of flowable fibre-reinforced concrete. *Eng. Struct.* **2016**, *124*, 186–195. [CrossRef]
23. Loukil, M.; Hassine, W.B.; Limam, O.; Experimental, P.K. Experimental determination of GFRC tensile parameters from three-point bending tests using an analytical damage model. *Constr. Build. Mater.* **2019**, *223*, 477–490. [CrossRef]
24. *ASTM C150*; Standard Specification for Portland Cement. American Society for Testing and Materials: West Conshohocken, PA, USA, 2018; pp. 1–9. [CrossRef]
25. *ASTM C33*; Standard Specification for Concrete Aggregates. American Society for Testing and Materials: West Conshohocken, PA, USA, 2016. [CrossRef]
26. Chu, H.; Gao, L.; Qin, J.; Jiang, J.; Wang, D. Mechanical properties and microstructure of ultra-high-performance concrete with high elastic modulus. *Constr. Build. Mater.* **2022**, *335*, 127385. [CrossRef]
27. *ASTM C1611*; Standard Test Method for Slump Flow of Self-Consolidating Concrete. American Society for Testing and Materials: West Conshohocken, PA, USA, 2018. [CrossRef]
28. *C138/C138M-17a*; Standard Test Method for Density (Unit Weight), Yield, and Air Content (Gravimetric) of Concrete. American Society for Testing and Materials: West Conshohocken, PA, USA, 2017. [CrossRef]
29. *ASTM C39/C39M-17a*; Standard Test Method for Compressive Strength of Cylindrical Concrete Specimens. American Society for Testing and Materials: West Conshohocken, PA, USA, 2017. [CrossRef]
30. *ASTM C215*; Standard Test Method for Fundamental Transverse, Longitudinal, and Torsional Resonant Frequencies of Concrete Specimens. American Society for Testing and Materials: West Conshohocken, PA, USA, 2002. [CrossRef]
31. *ASTM E 1876*; Standard Test Method for Dynamic Young's Modulus, Shear Modulus, and Poisson's Ratio by Impulse Excitation of Vibration. American Society for Testing and Materials: West Conshohocken, PA, USA, 2015; pp. 1–15. [CrossRef]

32. *ASTM C469*; Standard Test Method for Static Modulus of Elasticity and Poisson's Ratio of Concrete in Compression. American Society for Testing and Materials: West Conshohocken, PA, USA, 2014; pp. 1–5. [CrossRef]
33. *ASTM C157*; Standard Test Method for Length Change of Hardened Hydraulic-Cement Mortar and Concrete. American Society for Testing and Materials: West Conshohocken, PA, USA, 2017. [CrossRef]
34. *ASTM C1581*; Standard Test Method for Determining Age at Cracking and Induced Tensile Stress Characteristics of Mortar and Concrete under Restrained Shrinkage. American Society for Testing and Materials: West Conshohocken, PA, USA, 2009. [CrossRef]
35. Du, L.; Folliard, K.J. Mechanisms of air entrainment in concrete. *Cem. Concr. Res.* **2005**, *35*, 1463–1471. [CrossRef]
36. Chung, D.D. Dispersion of Short Fibers in Cement. *J. Mater. Civ. Eng.* **2005**, *17*, 379–383. [CrossRef]
37. Sanjeev, J.; Nitesh, K.J.N.S. Study on the effect of steel and glass fibers on fresh and hardened properties of vibrated concrete and self-compacting concrete. *Mater. Today Proc.* **2020**, *27*, 1559–1568. [CrossRef]
38. Hake, S.L.; Shinde, S.S.; Bhandari, P.K.; Awasarmal, P.R.; Kanawade, B.D. Effect of Glass Fibers on Self Compacting Concrete. *E3S Web Conf.* **2020**, *170*, 1–6. [CrossRef]
39. Ahmad, S.; Umar, A.; Masood, A. Properties of Normal Concrete, Self-compacting Concrete and Glass Fibre-reinforced Self-compacting Concrete: An Experimental Study. *Procedia Eng.* **2017**, *173*, 807–813. [CrossRef]
40. Güneyisi, E.; Atewi, Y.R.; Hasan, M.F. Fresh and rheological properties of glass fiber reinforced self-compacting concrete with nanosilica and fly ash blended. *Constr. Build. Mater.* **2019**, *211*, 349–362. [CrossRef]
41. Mehdipour, I.; Libre, N.A.; Shekarchi, M.; Khanjani, M. Effect of workability characteristics on the hardened performance of FRSCCMs. *Constr. Build. Mater.* **2013**, *40*, 611–621. [CrossRef]
42. Ghosh, D.; Abd-Elssamd, A.; Ma, Z.J.; Hun, D. Development of high-early-strength fiber-reinforced self-compacting concrete. *Constr. Build. Mater.* **2021**, *266*, 121051. [CrossRef]
43. Concrete, S.C. The European guidelines for self-compacting concrete. *BIBM, et al* **2005**, *22*, 563.
44. Yousefieh, N.; Joshaghani, A.; Hajibandeh, E.; Shekarchi, M. Influence of fibers on drying shrinkage in restrained concrete. *Constr. Build. Mater.* **2017**, *148*, 833–845. [CrossRef]
45. Kumar, D.; Rex, L.K.; Sethuraman, V.S.; Gokulnath, V.; Saravanan, B. High performance glass fiber reinforced concrete. *Mater. Today Proc.* **2020**, *33*, 784–788. [CrossRef]
46. Aslani, F.; Nejadi, S. Self-compacting concrete incorporating steel and polypropylene fibers: Compressive and tensile strengths, moduli of elasticity and rupture, compressive stress–strain curve, and energy dissipated under compression. *Compos. Part B Eng.* **2013**, *53*, 121–133. [CrossRef]
47. Rambo, D.A.S.; de Andrade Silva, F.; Filho, R.D.T. Mechanical behavior of hybrid steel-fiber self-consolidating concrete: Materials and structural aspects. *Mater. Des.* **2014**, *54*, 32–42. [CrossRef]
48. Abdullah, M.M.; Jallo, E.K. Mechanical properties of glass fiber reinforced concrete. *Al-Rafidain Eng. J. (AREJ)* **2012**, *20*, 128–135. [CrossRef]
49. Kizilkanat, A.B.; Kabay, N.; Akyüncü, V.; Chowdhury, S.; Akça, A.H. Mechanical properties and fracture behavior of basalt and glass fiber reinforced concrete: An experimental study. *Constr. Build. Mater.* **2015**, *100*, 218–224. [CrossRef]
50. Barluenga, G.; Hernández-Olivares, F. Cracking control of concretes modified with short AR-glass fibers at early age. Experimental results on standard concrete and SCC. *Cem. Concr. Res.* **2007**, *37*, 1624–1638. [CrossRef]
51. Messan, A.; Ienny, P.; Nectoux, D. Free and restrained early-age shrinkage of mortar: Influence of glass fiber, cellulose ether and EVA (ethylene-vinyl acetate). *Cem. Concr. Compos.* **2011**, *33*, 402–410. [CrossRef]